X-ray tomography characterization of fracture surfaces during dissolution

Philippe Gouze, Catherine Noiriel,[1] Céline Bruderer, Didier Loggia, and Richard Leprovost

Laboratoire de Tectonophysique, ISTEEM, CNRS-Université de Montpellier 2, Montpellier, France

Received 11 December 2002; accepted 28 January 2003; published 15 March 2003.

[1] The changes of fracture surfaces geometry and extend are studied using X-ray tomography during aperture increase due to CO_2-rich fluid percolation. Dissolution experiments were conducted on two micritic rock samples; one pure calcite end-member and one with typical composition for marine carbonates (85% calcite). High-resolution digital images of the fracture geometry allow quantifying the surface properties changes over four spatial scales with a resolution of 4.91 μm. Fracture surfaces are self-affine with an initial dimension of 2.5. Dissolution of the pure-calcite sample is clearly a process of homogeneous chemical "erosion" of the surface elevation: fractal dimension and specific surface remains constant (1.5 times the planar surface). Conversely, for the 85% calcite sample, initial topographic surfaces of the fracture walls evolve rapidly toward "non-topographic" interfaces displaying overhangs due the preferential dissolution of the carbonate grains. In this case, the conventional definition of the effective aperture must be revisited. Such structures can only be assessed from 3D observations. As dissolution progresses, the specific surface increases strongly, more than 5 times the planar surface, and probably faster than the reactive surface. *INDEX TERMS:* 5104 Physical Properties of Rocks: Fracture and flow; 5139 Physical Properties of Rocks: Transport properties; 5114 Physical Properties of Rocks: Permeability and porosity; 5112 Physical Properties of Rocks: Microstructure; 5194 Physical Properties of Rocks: Instruments and techniques. **Citation:** Gouze, P., C. Noiriel, C. Bruderer, D. Loggia, and R. Leprovost, X-ray tomography characterization of fracture surfaces during dissolution, *Geophys. Res. Lett.*, *30*(5), 1267, doi:10.1029/2002GL016755, 2003.

1. Introduction

[2] Limestone aquifers constitute a major reserve of fresh water throughout the world. Fractures, which develop in low permeability rocks, are the principal path for water flow and contamination. An increasing number of studies is devoted to understand the physics of flow and transport in fracture networks [e.g., *Adler and Thovert*, 1999]. For a connected fracture network, large-scale flow and hydrodispersive transport is first controlled by the geometrical properties of the individual fractures. In addition to fracture aperture, surface roughness and aperture tortuosity are usually put forward as the key parameters that control flow type and dispersion regime [*Brown et al.*, 1998; *Detwiler et al.*, 2000; *Glover et al.*, 1997]. Measurements of spatial distribution changes of the fracture aperture in the course of dissolution were achieved only recently [*Dijk et al.*, 2002; *Durham et al.*, 2001], producing important constraints for modelling flow and dissolution patterns. Large uncertainties still remain on the relation that links the macroscopic evolution of the aperture and the microscopic (grain scale) morphological evolution of the fracture walls that controls fluid-rock fluxes.

[3] For smooth laminar flow, velocity distribution across the fracture section is parabolic, $u(z) = u_0(1 - 4z^2/a^2)$, where u_0 is the maximum velocity and a is the aperture. The aperture-scale Péclet number, Pe, denotes the ratio of the characteristic time for transverse homogenization by diffusion $a^2/4D_m$, to the mean longitudinal residence time $a/2\langle u\rangle_z$, where $\langle u\rangle_z$ is the fracture-section averaged velocity ($\langle u\rangle_z = 2/3\ u_0$). If $Pe \gg 1$, Taylor-Aris dispersion approximation holds with the longitudinal dispersion D_L proportional to Pe^2 [*Detwiler et al.*, 2000]. It is then possible to analyse processes in term of resident concentration of a solute, $\langle c_i\rangle_z = \int_a c_i dz$. Far from equilibrium, the change in the concentration is controlled by the hydrodispersive transport (embodied in the differential operator $\mathbf{J}(\langle c_i\rangle_z)$), the adimensional saturation index $I(\langle c_i\rangle_z) \sim 1 - \langle c_i\rangle_z/c_i^*$ (where c_i^* is the equilibrium concentration), the kinetic mass transfer rate constant k_r, and the extend of the contact area between the fluid and the rock (inhibiter-catalyser effects are not taken into account). With A_R the reactive area by unit fluid volume, macroscopic balance equation for small variation of species i concentration, $\langle c_i\rangle_z$, is [*Lasaga*, 1998]:

$$\partial\langle c_i\rangle_z/\partial t = \mathbf{J}(\langle c_i\rangle_2) + A_r k_r I(\langle c_i\rangle_z) \quad (1)$$

Recognizing that k_r is an intrinsic property of the considered reaction for a given pH profile, temporal change of the dissolution rate is controlled by both the change in A_R and a. The reciprocal effects of aperture variability changes on dissolution were investigated through different numerical approach by *Békri et al.* [1997], *Dijk and Berkowitz* [1998] and *Hanna and Rajaram* [1998]. In these works, the evolution of A_r was not taken into account. Indeed, measuring A_r is challenging. Even the description of the effective reactive area for polycrystalline altered rocks in relation to the one of the pure phase used in experimental determination of k_r in batch reactor is debated [e.g., *Gautier et al.*, 2001]. Alternatively, assuming $\mathbf{J}(c_i)$ known, the product $A_R k_r$ can be evaluated from (1), measuring the difference in reactant concentration between the outlet and the inlet [*Kieffer et al.*, 1999]. However, providing that continuous measurement of such low concentration is possible, results reflect only averaged values A_R. To progress toward a full

[1] Also at CIG, Ecole des Mines, Fontainbleau, France.

0094-8276/03/2002GL016755$05.00

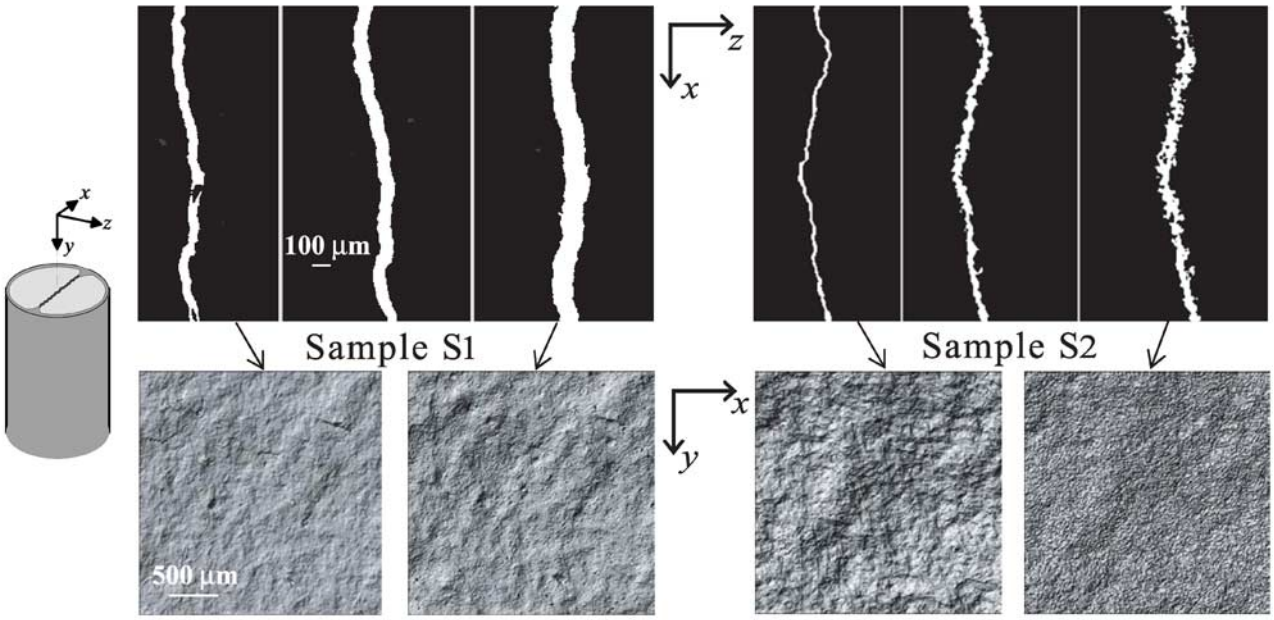

Figure 1. Top: binarised CMT cross-section (y = 6 mm) of the fracture (left: before dissolution, middle: an intermediary stage and right: final stage. Bottom: 512^2 pixel projection of the upper fracture wall before dissolution (left) and at the final stage post-dissolution (right).

spatio-temporal quantification of the fracture properties, we present here a study based on X-ray tomography using the European Synchrotron Radiation Facility (ESRF). For this first attempt, we measure the changes of aperture and fracture walls geometry at different stages of kinetic-controlled dissolution due to flow of acidic water.

2. Experimental Method

[4] Two samples S1 and S2 of cretaceous limestone cored from the same borehole are studied. S1 is composed of ~100% calcite (clay <1 w%) with 2.2% porosity. S2, is composed of 85 w% calcite, 10 w% dolomite, 5 w% clay with 5.6% porosity. Mini-cores of 6 mm diameter and 12 mm long were prepared to suit the optimal size for the ESRF-ID19 X-ray beam for non-local computed micro-tomography (CMT). A tensile fracture, sub-collinear to the core axis, was made. Then, the mini-cores were coated with epoxy to avoid any mechanical deformation during the percolation experiment.

[5] We use a 2048^2 pixels camera, with an effective pixel size of 4.91 μm. This setup allows a very intense monochromatic X-ray beam of $10mm^2$. Finally a 3D X-ray absorption image is computed from 900 radiographies acquired at every 0.2 degree of view angle. A bimodal segmentation algorithms based on challenge region growing allows individualizing the fracture volume.

[6] Dissolution is obtained by flowing, at a constant rate of $2.8\ 10^{-9}\ m^3.s^{-1}$, pure water enriched with CO_2 at partial pressure of 0.1 MPa ($pH = 4 \pm 0.1$). Output pH is 5.1 ± 0.15. The effect of confining pressure (equal to the max pressure at the inlet) variation was negligible. The pressure at the outlet was maintained above 0.1 MPa in order to avoid CO_2 degassing in the mini-core. Because of the constant rate injection, Pe remains constant during the dissolution at value of ~440.

3. Results and Analyses

[7] Let define the adimensional reaction surface coefficient as $S_R = A_R \langle a \rangle/2$. At the initial stage, S_R is estimated as the product of the volume fraction of the mineral involved in the given reaction, by the specific surface coefficient S_S which denotes the tortuosity of the fracture walls (S_S = 1 for a planar surface). It is assumed here that the fracture intersects the rock randomly. Usually, for numerical modeling, S_R is kept constant and S_S is initially evaluated and embedded in an "efficient" kinetic reaction rate [*Lasaga*, 1998]. The validity of this relation in the course of dissolution is questionable: we will see later that (i) S_S may change strongly during dissolution and (ii) the ratio S_R/S_S is probably non-constant in the case of non-pure calcite, due to preferential dissolution.

3.1. Fracture Walls and Aperture Changes

3.1.1. The Initial Stage

[8] The initial mean aperture along the central flow axe is 50 μm (σ_a = 8 μm) for S1 and 20 μm (σ_a = 7 μm) for S2. For both samples, the initial fracture surfaces are topographic (hereafter reported as Topographic Surfaces; TS), that is, to any x-y coordinate corresponds a single elevation z. Then, fracture walls are first analyzed by extracting the x-y projection of the CMT images, producing profilometry-equivalent data set (Figure 1) to be characterized by classical statistical and spectral surface analysis. The area of a self-affine fractal surface increases with both its fractal dimension and σ_z^2 the variance of the surface elevation. Results display ubiquitous self-affine behaviour all over the measured scale range from 5 μm to 1 cm. The fractal

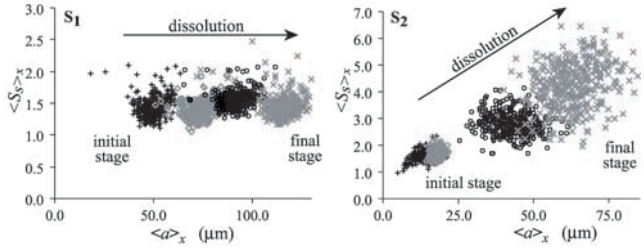

Figure 2. x-averaged specific surface coefficient $\langle S_S \rangle_x$ versus fissure aperture $\langle a \rangle_x$.

dimension $\boldsymbol{D}$ = 2.5 ± 0.1, computed coherently using 1D and 2D power spectrum method [e.g., *Schmittbuhl et al.*, 1995] is isotropic.

3.1.2. Evolution of S1

[9] The experiment consists of three dissolution steps with a mean aperture increase of 22 ± 2 μm for each of them. Dissolution of S1 appears as a uniform translation (chemical "erosion") of the x-y surfaces along the z axis. Both the fractal dimension $\boldsymbol{D}$, and the variance of the surface elevation σ_z^2 remain constant: fracture walls stay TS.

3.1.3. Evolution of S2

[10] The dissolution of S2 sample consists of three steps of variable duration (aperture increase of 4.5, 23 and 15 μm respectively). In contrast with S1, dissolution of S2 is noticeably heterogeneous. Cross sections of the final stage of the experiment (Figures 1 and 4c), show that fracture walls cannot be described anymore as TS (lets call it a Non-Topographic Surface or NTS). Note that the solid phase pixels (in black), are connected in 3D, so that the apparent isolated clusters on the cross sections reflect the 3D nature of the fracture walls. Indeed, where the surface is "folded", some x-y coordinate have several elevations z creating multiple overhangs and the analysis of 2D-projected digital images of the fracture walls is biased (Figure 4d). The surfaces were analysed using isomorphic 3D-box-counting method (BCM) and isomorphic/non-isomorphic 2D-BCM on the x-z cross-sections. All those methods give similar results: a linear relation between the logarithm of the number of boxes of dimension l and the logarithm of l. This indicates that the self-affine fractal characteristic of the surface remains. A theoretical value of the fractal dimension of the surfaces can be calculated from the slope s of the former linear trend by the relation $\boldsymbol{D}_{BCM} = -s$ for 3D-BCM and $\boldsymbol{D}_{BCM} = -s + 1$ for 2D-BCM. A value of $\boldsymbol{D}_{BCM}$ = 2.2 ± 0.1 was calculated for the fracture surfaces of S1 and S2 at the initial stage. $\boldsymbol{D}_{BCM}$ increases toward 2.4 ± 0.1 for the final stage of the dissolution of S2 whereas it stays at the initial value for S1. Albeit the noticeable, but expected [e.g., *Schmittbuhl et al.*, 1995], difference between the dimension measured by spectral methods and the BCM, the results reveal a quantifiable increase of the fractal dimension that comes together with an increase, of the variance of the surface σ_z^2 in the course of dissolution of S2.

3.2. Evolution of Specific Surface with Dissolution

[11] Specific surface coefficient $S_S(x, y)$ and fracture aperture $a(x, y)$ were measured from the 3D CMT images of S1 and S2. When fluid-rock interface is a NTS, $a(x, y)$ represents the cumulative aperture $a'(x, y)$ as explained on Figure 4b. Correlation between x-averaged $\langle S_S \rangle_x$ and $\langle a \rangle_x$ were measured on a 250 μm width stripe ($-125 < x < 125$ μm) in order to avoid boundary effects (Figure 2). Results show that the values of $\langle S_S \rangle_x$ increase from 1.5 to 5 for S2, whereas they remain constant around 1.5 for S1. For S1, the spreading of $\langle S_S \rangle_x$ data is unchanged from the beginning to the end of the experiment while the mean aperture increases of about 70 μm. Conversely, S2 displays an increase of the $\langle S_S \rangle_x$ data spreading with increasing dissolution (Figure 2). This scattering reflects the more and more localized dissolution, at micro-scale, observed on the cross sections (Figure 1).

4. Discussion and Conclusions

[12] The characteristic time τ_r for the dissolution reaction $CaCO_3 + H^+ \rightarrow Ca^{++} + HCO_3^-$ is $c_i^*/A_R k_r$. Applying (1) to the calcium concentration, c^* is equal to 8.5 mol.m^{-3} and k_r ranges from 6.3 10^{-5} mol.m^{-2}.s^{-1} at the input to 1.6 10^{-5} mol.m^{-2}.s^{-1} at the output (calculated from the $k_r - pH$ relation given by *Plummer et al.* [1978]). With $A_R = 2F_{Ca}S_S/a$, where F_{Ca} is the calcite fraction in the rock, τ_r ranges from 2.2 to 22 s in the case of S1 and from 1 to 6 s in the case of S2. Those values are comparable to the characteristic time for convection throughout the sample which range from 0.8 to 2.5 s as aperture increases. Disequilibrium occurs along the entire fracture length, under control of both the reaction kinetic and the convective transport (Damköhler number ranging from 1 to 10). As a consequence, quasi-uniform dissolution is observed (Figure 3), which corresponds to the case "typical Damköhler and typical Péclet" explored numerically by *Dijk and Berkowitz* [1998]. Equivalent situations were studied by *Mourzenko et al.* [1996] in the case of the deposition in self-affine fractures. From this macroscopically uniform dissolution, the present work shows that diverse complex microscopic patterns may arise from dissolution as soon as polycrystalline solids are concerned. The initial TS fluid-rock interface evolves rapidly towards NTS, which cannot be characterized using classical profilometry methods (roughness exponent, specific and reactive surfaces would be significantly underestimated).

[13] As a result of NTS development, the total specific surface increases strongly. However, the SEM observations reveal that the calcite specific surface or reactive surface may not increase in the same proportion: the increase of the total specific surface is mostly due to the increase of the exposed surface of the others mineral phases. Still, this increase cannot persist indefinitely and the exploration of longer dissolution time is necessary to study, the role of the mechanical ablation of the non-dissolved fraction. Presently,

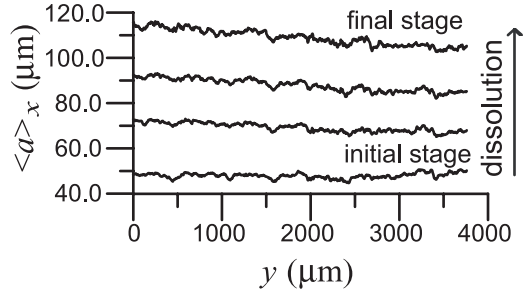

Figure 3. Aperture averaged on $-125 < x < 125$ μm as a function of distance to the input.

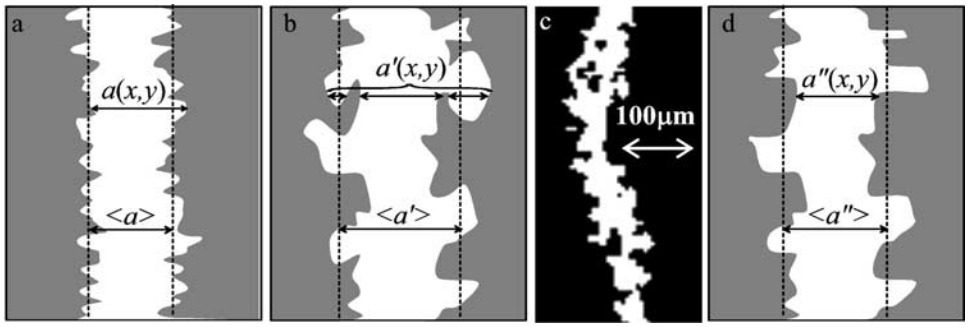

Figure 4. Schematic representation of TS (a) and NTS (b) to be compared to a magnification of the S2 fracture walls (c). (d) Axial plan projection of the NTS fracture wall as it would be measured using profilometry techniques.

it can be concluded from the apparently unconditional increase of S_S with a, that the relation between S_R and S_S is certainly non-linear because of the preferential dissolution of the carbonated phase. We demonstrated that the fracture surface were intrinsically self-affine fractal all over the large range accessible by this imaging method (λ_C = 4.91 μm). It is probable that this behaviour persists until the average grain size; λ_{GS} = 2 μm (evaluated from SEM observations). By definition the specific surface coefficient *Ss* is proportional to $(\lambda_C)^{2-\boldsymbol{D}}$. From this relation, and assuming that σ_z^2 is independent of the observation scale, one can extrapolate the maximum values of S_S as well as S_R and A_R from the values of $\boldsymbol{D}$. Replacing λ_C by λ_{GS} in the aforementioned relation, the maximum values of S_S for S1 and S2.are 2.4 and 9.5 respectively.

[14] When fractures walls become NTS, the definition of the aperture $a(x, y)$ becomes problematic (Figure 4) which may have strong implications on its use as a pertinent parameter for computing flow and transport processes. For example, the validity of the Hagen-Poiseuille cubic law, that link the permeability k to the square of the aperture of TS-type fracture has been discussed by many researchers, which broadly conclude that the principal factor causing deviation from ideal parallel plate theory is the non-smooth geometry of fracture: NTS complicates the discussion as a single definition the fracture aperture is no longer possible. It is generally admitted that the effective hydraulic aperture is the one that would give identical pressure drop in parallel plan geometry for a given flow rate. For low flow rate and assuming that the mean asperities height remains negligible compared to the mean aperture, the effective aperture is certainly closer to the axial plan ($x, y, z = 0$) projection of the real aperture ($a''(x, y)$ on Figure 4d) as it can be obtained using profilometry methods. The validity of this assertion for higher flow rate is questionable. More importantly, overhangs play probably an important role in the hydro-dispersive transport processes. The storage of solute in the dead-end zones increases the retardation factor for tracers and pollutants transport. Taking into account such structures in the course of dispersion processes is tricky and requires further investigations: the effective aperture probably depends on the dominant dispersion regime and ranges from the cumulative aperture, $a'(x, y)$, to the projected aperture $a''(x, y)$.

[15] To our knowledge, there is very little published work aiming to observe directly morphological changes in fracture. The most comparable one was proposed by *Durham et al.* [2001], although classical profilometry measurements were used requiring opening out the sample at each dissolution stage to have access to the fracture surfaces. As demonstrated here, X-ray computed tomography is an efficient non-invasive measurement tool for investigating the variability of fracture geometrical properties and its changes due to chemically induced dissolution of the mineral phases.

[16] **Acknowledgments.** We thank E. Boller and P. Cloetens (ESRF) and D. Bernard (ICMCB) for their help in processing the data. Research supported by the European Commission RDG (EVK1-CT-2001-00091/ ALIANCE).

References

Adler, P. M., and J. F. Thovert, Fractures and fractures networks, Kluwer Acad., Norwell, Mass., 1999.

Békri, S., J. F. Thovert, and P. M. Adler, Dissolution and deposition in fractures, *Eng. Geol.*, *48*, 283–308, 1997.

Brown, S., A. Caprihan, and R. Hardy, Experimental observation of fluid flow channels in a single fracture, *J. Geophys. Res.*, *103*, 5125–5132, 1998.

Detwiler, R. L., H. Rajaram, and R. J. Glass, Solute transport in variable-aperture fractures: An investigation of the relative importance of Taylor dispersion and macrodispersion, *Water Resour. Res.*, *36*, 1611–1625, 2000.

Dijk, P. E., and B. Berkowitz, Precipitation and dissolution of reactive solutes in fractures, *Water Resour. Res.*, *34*, 457–470, 1998.

Dijk, P. E., B. Berkowitz, and Y. Yechieli, Measurement and analysis of dissolution patterns in rock fractures, *Water Resour. Res.*, *38*, 5–11, 2002.

Durham, W. B., W. L. Bourcier, and E. A. Burton, Direct observation of reactive flow in a single fracture, *Water Resour. Res.*, *37*, 1–12, 2001.

Gautier, J.-M., E. H. Oelkers, and J. Schott, Are quartz dissolution rates proportional to B. E. T. surface areas?, *Geochim. Cosmochim. Acta*, *65*, 1059–1070, 2001.

Glover, P. W. J., K. Matsuki, R. Hikima, and K. Hayaashi, Fluid flow in fractally rough synthetic fractures, *Geophys. Res. Lett.*, *24*, 1803–1806, 1997.

Hanna, R. B., and H. Rajaram, Influence of aperture variability on dissolutional growth of fissures in karts formations, *Water Resour. Res.*, *34*, 2843–2853, 1998.

Kieffer, B., C. F. Jové, E. H. Oelkers, and J. Schott, An experimental study of the reactive surface area of Fontainebleau sandstone as a function of porosity, permeability, and fluid flow rate, *Geochim. Cosmochim. Acta*, *63*, 3525–3534, 1999.

Lasaga, A. C., Kinetic theory in the earth sciences, Princeton Univ. Press, Princeton, N. J., 1998.

Mourzenko, V. V., S. Békri, J.-F. Thovert, and P. M. Adler, Deposition in fractures, *Chem. Eng. Comm.*, *148–150*, 431–464, 1996.

Plummer, N., T. M. L. Wigley, and D. L. Parkhurst, The kinetic of calcite dissolution in CO_2-water systems at 5° to 60°C and 0 to 1 atm CO_2, *Am. J. Sci.*, *278*, 179–216, 1978.

Schmittbuhl, J., J. P. Vilotte, and S. Roux, Reliability of self-affine measurements, *Phys. Rev., E*, *51*, 131–147, 1995.

C. Bruderer, P. Gouze, R. Leprovost, D. Loggia, and C. Noiriel, Laboratoire de Tectonophysique (ISTEEM), 34095, Montpellier cédex 5, France. (philippe@msem.univ-montp2.fr)